

Microstructural heterogeneity in hexagonal close-packed pure Ti processed by high-pressure torsion

Y. J. Chen · Y. J. Li · J. C. Walmsley ·
N. Gao · H. J. Roven · M. J. Starink ·
T. G. Langdon

Abstract Microstructural evolution was studied quantitatively by electron backscattering diffraction in commercial purity Ti processed by high-pressure torsion (HPT) at room temperature. The results show that a heterogeneous microstructure develops during HPT processing with regions of both nanocrystalline grains (100 nm) and coarse grains ($\sim 1\text{--}30\ \mu\text{m}$). Tensile $\{10\bar{1}2\}$ twins were observed in the center of the disk after the first turn of HPT. The microhardness near the disk center increases with increasing HPT turns and the hardness after 5 turns is reasonably homogeneous at radial positions [1 mm]. The mechanism of grain refinement is characterized by dynamic recrystallization and the continuous formation of a necklace-like array of fine grains gradually consumes the larger grains in subsequent passes.

Y. J. Chen (&) · H. J. Roven
Department of Materials Science and Engineering,
Norwegian University of Science and Technology,
Alfred Getz vei 2B, 7491 Trondheim, Norway
e-mail: happywinner01@gmail.com

Y. J. Li · J. C. Walmsley
SINTEF Materials and Chemistry,
7465 Trondheim, Norway

N. Gao · M. J. Starink · T. G. Langdon
Materials Research Group, School of Engineering Sciences,
University of Southampton, Southampton SO17 1BJ, UK

T. G. Langdon
Departments of Aerospace & Mechanical Engineering
and Materials Science, University of Southern California,
Los Angeles, CA 90089-1453, USA

Experimental procedure

Grade 2 CP Ti was used in the rolled and annealed condition with an initial average grain size of $\sim 23 \pm 3\ \mu\text{m}$. This material is of interest because of the potential use in

Introduction

High pressure torsion (HPT) is a well-known procedure for obtaining bulk ultrafine-grained (UFG) and nanostructured metals (NSM) [1–4]. There has been significant progress in using HPT to fabricate nanostructured face-centered cubic (fcc) and body-centered cubic (bcc) metals, for example Al [2], Cu [3] and Ni [4] alloys and pure W [5], with average grain sizes less than 100 nm. By contrast, there has been less progress with hexagonal close-packed (hcp) materials. Although several investigations have demonstrated significant grain refinement by HPT processing using hcp metals, as with Mg [6], Ti [7–10] and Zr [11], the reported average grain sizes are generally above the transitional value of 100 nm which delineates nanostructured materials. Therefore, grain refinement in hcp metals appears to be less effective than in fcc and bcc materials.

Recent studies reveal that rather heterogeneous microstructures are obtained in hcp metals and their alloys when processing by HPT [6, 11, 12]. There are reports of heterogeneity in hcp Zr alloys after 1 turn of HPT with grains of $\sim 100\ \text{nm}$ and coarser micrometer-sized grains [11] and a bimodal microstructure in pure Mg processed by 5 turns of HPT [6]. The mechanisms for the formation of this unique microstructural feature in hcp materials are not yet clear. Most of the reports on hcp microstructures processed by HPT are based on using transmission electron microscopy (TEM) [6, 11, 12] which provides only limited information over relatively restricted areas. In order to achieve a representative overview of large areas of the samples, other characterization methods are needed. Accordingly, the present investigation was initiated on commercial purity (CP) Ti processed by HPT and using high resolution electron backscattering diffraction (EBSD) in a field emission gun scanning electron microscope (FESEM) to provide a more detailed characterization of the microstructure.

medical implants [14, 15]. Disks having diameters of 10 mm and thicknesses of 0.8 mm were processed by quasi-constrained HPT [4] for 1 and 5 turns at room temperature using a rotation speed of 1 rpm and an imposed pressure of 6.0 GPa. Figure 1 shows the radial (RD), transverse (TD) and normal directions (ND) and planes of

the deformed disks after HPT.

EBSD characterization was conducted in both the torsion plane (RD–TD) and longitudinal planes (RD–ND and TD–ND). Sample surfaces were prepared by electropolishing with A3 electrolyte, provided by Struers Ltd., Denmark. The EBSD mapping was performed in a Zeiss Supra SEM with step sizes of 500 and 100 nm for the 1- and 5-turn samples, respectively. The 5-turn sample was annealed at 523 K for 1 h before EBSD in an attempt to remove some of the residual stress and thereby to improve the quality of the Kikuchi diffraction patterns. TEM samples were cut from positions 3 mm from the disk center in the torsion plane (RD–TD) and subsequently mechanically thinned to 100 μm followed by double jet polishing in a solution containing 60% methanol, 35% butanol and 5% perchloric acid at 243 K with an electrode voltage of 40 V. TEM images were obtained using a Philips CM30 TEM operating at 200 kV. The Vickers microhardness was measured across the diameter of each disk using a load of 500 g and a dwell time of 15 s.

Experimental results and discussion

Typical microstructures after HPT are shown in Fig 2a–d. The color code, red for $\{0001\}$, blue for $\{10\bar{1}0\}$ and green for $\{2\bar{1}10\}$, gives the orientation of each grain in the EBSD image. Figure 2a shows the initial microstructure in the center of the torsion plane after 1 turn of HPT where the

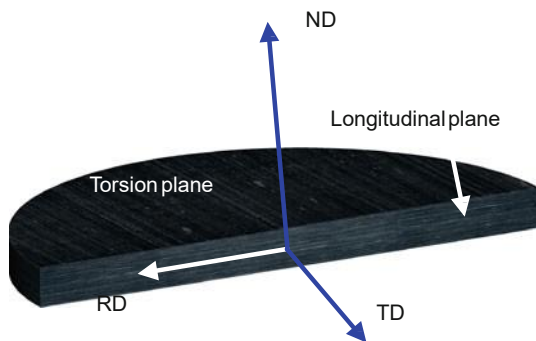


Fig. 1 Definition of the observational directions and planes

grains are reasonably equiaxed indicating that there is only limited shear deformation in the center of the disk [16]. One distinctive feature is the presence of a high fraction of $\{10\bar{1}2\}$ tensile twins, corresponding to 86° $h\bar{1}\bar{2}10i$ twin boundaries. This suggests that the disk center is subjected primarily to severe compression. By contrast, Fig. 2b shows that the coarse grains at a position of 3 mm from the disk center are heavily elongated and refined. Specifically, large numbers of fine necklace-like grains and deformation bands (DBs) are formed along the grain boundaries and within some of the coarser grains, respectively. Unlike the disk center, most of these grains have become reoriented with the $\{0001\}$ crystal planes aligned parallel to the torsion plane thereby showing that the deformation texture is caused mainly by shear deformation during torsion. The fraction of twins in Fig. 2b is 2.2% which is much lower than the fraction of 34.4% in the center of the disk in Fig. 2a so that the dominant deformation mechanism is dislocation slip rather than deformation twinning. This is reasonable because $\{10\bar{1}2\}$ deformation twinning can accommodate only ~ 0.12 shear strain [17].

The microstructure was also investigated in the longitudinal plane section as shown in Fig. 1. Figure 2c shows that the grains in the longitudinal plane (TD–ND) seem larger than those in the torsion plane at the same distance from the disk center and this suggests that there is a deformation gradient through the thickness of the disk. Similar to the same location in the torsion plane (RD–TD), parallel DBs and elongated coarse grains are the main features at this strain. The fine-grained region tends to form at the junction of grain boundaries or tips of DBs. One interesting feature, which contrasts with the microstructure in Fig. 2b, is the $\{0001\}$ basal planes (red color) almost lacking in this observation.

For the HPT 5-turn samples, it was not possible to obtain good Kikuchi patterns to permit mapping over all parts of the sample even after annealing at 523 K. Nevertheless, coarse grains were also observed having sizes in the range of $\sim 1\text{--}30$ μm . A typical heterogeneous microstructure in the longitudinal section at a radial position of 3 mm from the disk center is shown in Fig. 2d. It should be noted that some of the grains in the fine-grained region (~ 1 μm) marked in Fig. 2d may have non-indexed pixels (confidence index (CI) ~ 0.1) because of the poor quality of the Kikuchi patterns associated with heavy deformation (the fraction of indexing points in Fig. 2d is 72.1%, CI ≥ 0.1). However, the CI values for the coarse grains are high and these coarse grains are a real feature in the microstructure. It is believed that the coarser grains are not formed by grain coarsening during the short annealing at 523 K because this annealing temperature is too low for static recrystallization. This was confirmed by differential

scanning calorimetry where no recrystallization peaks were observed below 623 K and by noting an absence of any hardness reduction after annealing at 523 K.

Figure 3 shows TEM images of the grain structure at the surface of the torsion plane at 3 mm from the disk center after 1 and 5 turns of HPT. Figure 3a shows details of the fine-grained regions with grain size below 100 nm formed at the first turn of HPT. The corresponding selected area

diffraction (SAD) pattern further confirms the formation of the ultra-fine grains. Figure 3b shows a typical TEM image of the grain structure after 5 turns of HPT which further confirms the existence of the heterogeneous microstructure consisting of both coarse and fine grains. The grains in the nanocrystalline regions have a grain size below 100 nm while the coarse grains having sizes of [1 μm. The coarse grain in the upper part of Fig. 3b shows a contrast

Fig. 2 EBSD orientation maps a at the disk center in the torsion plane (RD–TD) after 1 turn of HPT, b at 3 mm from the center in the torsion plane after 1 turn of HPT, c at 3 mm from the disk center in the longitudinal plane (TD–ND) after 1 turn of HPT, d at 3 mm from disk center in the longitudinal plane (RD–ND) after 5 turns of HPT (Color figure online)

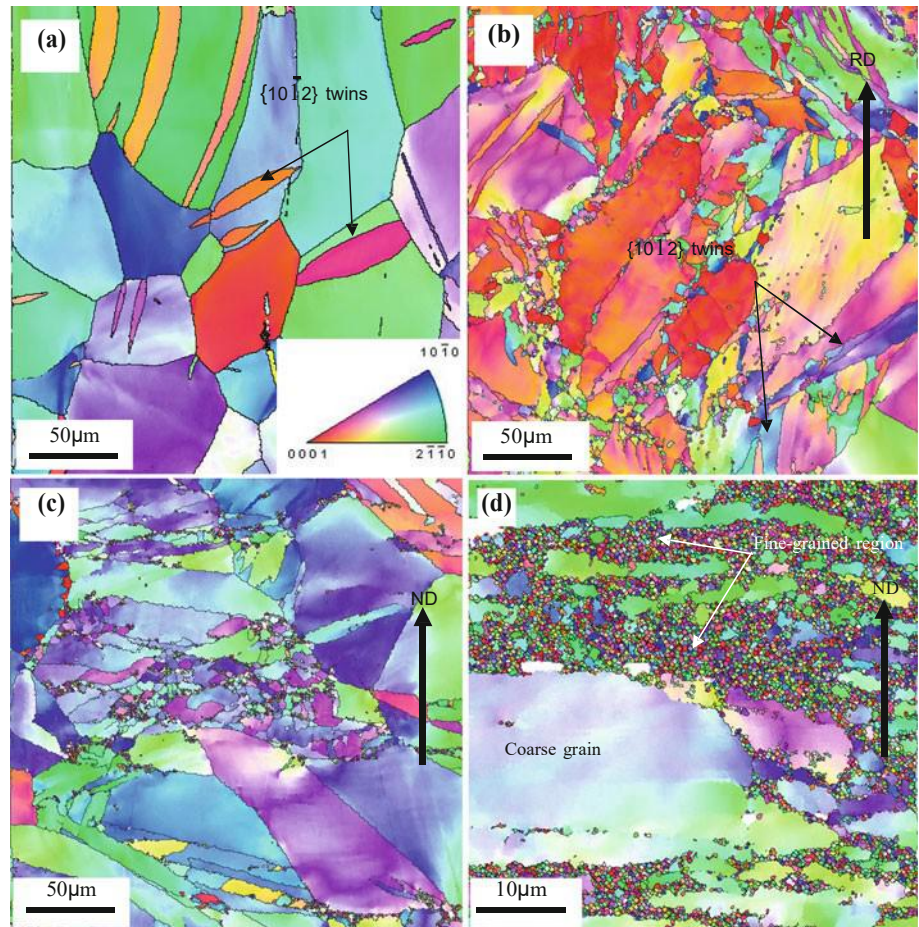


Fig. 3 TEM images at the surface of the torsion plane 3 mm from the disk center after a 1 turn of HPT (with SAD as an insert) and b 5 turns of HPT

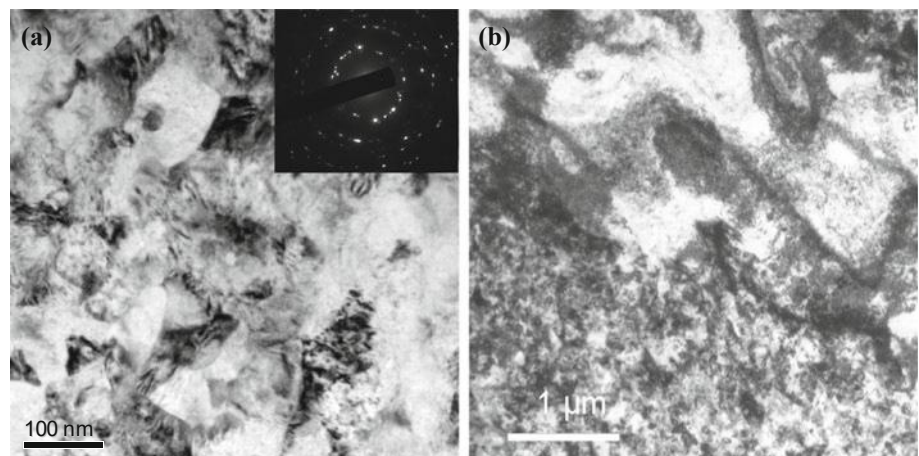
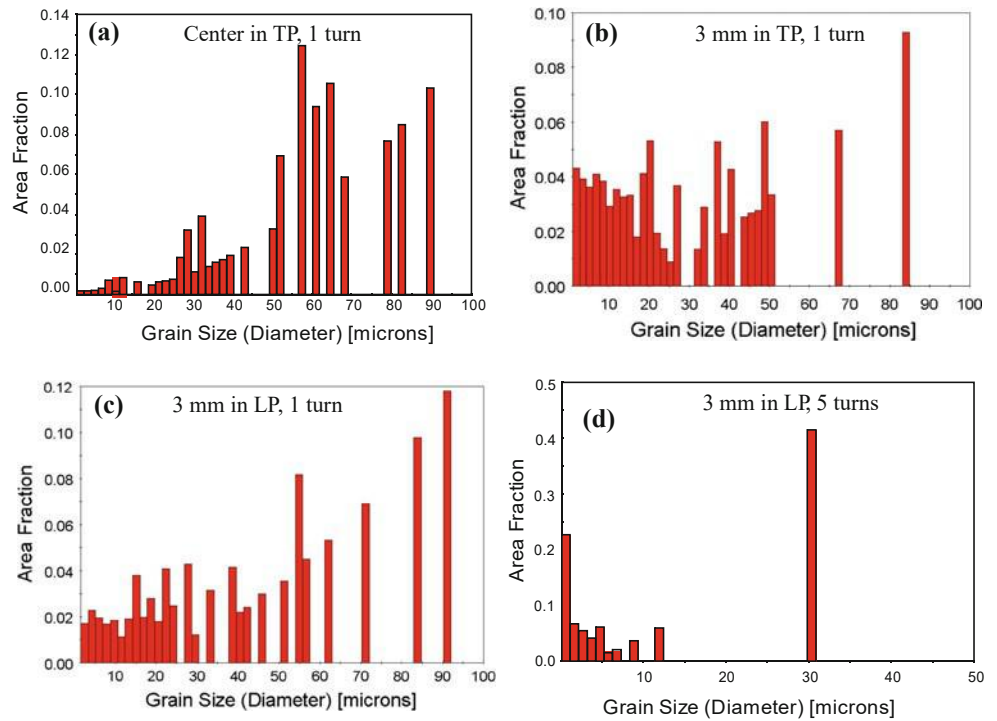


Fig. 4 Grain size distributions after 1 turn of HPT a at center of the torsion plane (TP), b at 3 mm from disk center in the TP, c at 3 mm from disk center in the longitudinal plane (LP), and d at 3 mm from disk center in the longitudinal plane after 5 turns of HPT



consistent with high levels of plastic deformation in the form of bend contours and a high dislocation density.

The grain size distributions (equivalent circle diameter) after HPT calculated from the EBSD images (Fig. 2) are given in Fig. 4. Figure 4a shows that the initial grain size is in a large range and the maximum grain size is around 90 μm . After shear strain of 1 turn HPT, it is apparent from Figure 4b and c that the fraction of fine grains is significantly higher at a distance of 3 mm from the center of the disk both in the torsion plane and in the longitudinal plane, although the maximum size of the coarse grains is similar to that of the initial microstructure, Figs.4a–c. Careful EBSD measurements along a radius in the torsion plane revealed a gradual refinement in the microstructure from the disk center to the periphery where this is consistent with the continuous increase in shear strain with distance from the center [16]. The grain size at the torsion surface in Fig. 4b is smaller than in the longitudinal plane in Fig. 4c indicating also a through-thickness heterogeneity. After 5 turns of HPT in Fig. 4d, the microstructure remained heterogeneous but with a significantly reduced range of grain sizes.

Fig. 5 shows the misorientation distributions of the high-angle grain boundaries (larger than 150°) after 1 and 5 turns. These distributions exhibit an obvious peak at 86° which is due to the presence of the $\{10\bar{1}2\}$ $\bar{h}\bar{1}011i$ tensile twins illustrated in Fig. 2. However, there is no detectable peak at 56° showing that $\{10\bar{1}1\}$ $h10\bar{1}2i$ compression twinning is not activated. Furthermore, the fraction of twins decreases with increasing strain, which is clearly

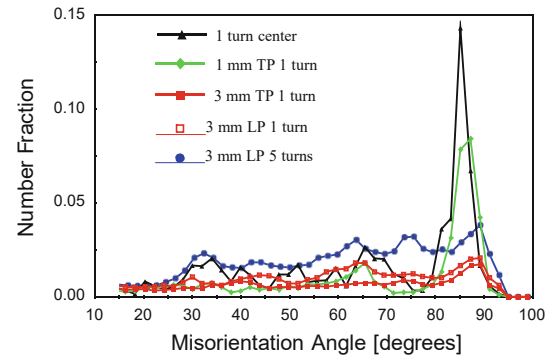


Fig. 5 Misorientation distributions observed after 1 and 5 turns

seen from the peak values of the disk center to 1 and 3 mm from the disk center of 1 turn HPT. Inspection shows the curve of the 1-turn HPT sample in the disk center also shows weak peaks at 65° and 35° corresponding to the $\{11\bar{2}2\}$ $h1\bar{1}2\bar{3}i$ compressive twins and $\{11\bar{2}1\}$ $\bar{h}\bar{1}126i$ tensile twins, respectively. These two twinning systems are usually activated at high stress levels [18].

It was reported earlier that a small fraction of $\{10\bar{1}2\}$ twins is activated in CP Ti during ECAP at 673 K [13] but these twins have not been reported in CP Ti after HPT. The $\{10\bar{1}2\}$ tensile twinning activated during the initial low strain deformation stage in this study shows that the twinning in HPT is different from ECAP where $\{10\bar{1}1\}$ twins are the most frequent twinning system operating at both elevated temperatures [19, 20] and room temperature

[21]. It is well known that the $\{10\bar{1}2\}$ twin represents the most active twinning mode for Ti during deformation at room temperature [18, 19] where the $\{10\bar{1}2\}$ system is activated by tension along the c-axis. Figure 2a shows that most grains in the disk center have the $\{0001\}$ basal planes perpendicular to the observation plane which is favorable for the activation of tensile $\{10\bar{1}2\}$ twins by severe compression. Hence, the texture existing in the disk center may explain the presence of a high fraction of $\{10\bar{1}2\}$ tensile twins in the present experiments.

The Vickers microhardness measurements across the diameters of the HPT samples are shown in Fig. 6. The microhardness in the unprocessed condition is reasonably uniform but several trends are visible after HPT. First, the microhardness increases significantly on both the torsion and the longitudinal planes after 1 turn and the microhardness is consistently higher in the torsion plane than in the longitudinal plane which is consistent with the microstructures in Figs 2b and c. Second, the microhardness increases with distance from the center to the periphery and

a more homogeneous distribution is obtained after 5 turns which is consistent with earlier results for pure Ti after HPT [8]. Third, the microhardness near the disk center increases with increasing HPT turns as predicted by the accumulation of geometrically-necessary dislocations due to the large strain gradient induced by HPT [22] and by strain gradient plasticity modeling [23]. Fourth, the hardness after 5 turns is reasonably homogeneous at radial positions [1 mm implying that grain refinement has reached an essentially saturated condition. This is reasonable because it is well established that 5 turns of HPT is generally sufficient to obtain reasonable homogeneity in many materials [24–26]. Finally, it is noted that the imposed pressure of 6.0 GPa in these experiments is sufficiently high that there will be no significant slipping during HPT processing [27].

The present study shows that the processed microstructure at high strain (5 turns) is heterogeneous in nature. After substantial deformation by HPT at room temperature, the microstructure consists of regions of nanocrystalline grains (100 nm) and other regions of coarser grains (*1–30 μ m). This inhomogeneous microstructure is different from fcc and bcc metals for which the microstructural change is more homogeneous [2–5]. This also contrasts with the same material processed by ECAP at high temperature (723 K) where there was a homogeneous UFG microstructure [28]. The difference is thought due to the limited number of slip systems, the high critical shear stress for slip in hcp Ti at room temperature and the one-directional shear deformation during HPT. As is apparent in Fig. 7a, the coarse grains after 5 turns of HPT have very limited internal low angle grain boundaries (LAGBs, misorientations from 1.5° to 15°) and they show no evidence of twinning. The absence of deformation twins (Fig. 7a) and formation of coarse scale dislocation structures (Fig. 3b) may suggest that the deformation by dislocation slip in these coarse grains is enough to accommodate

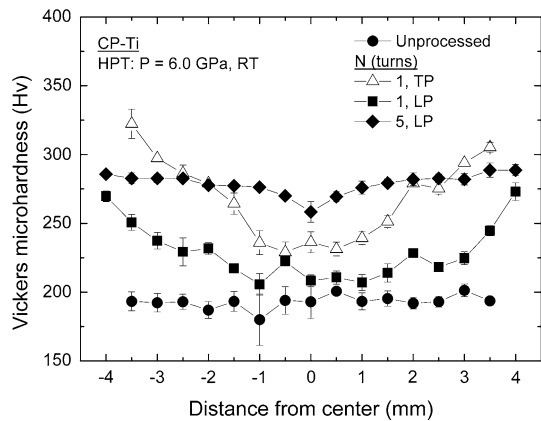
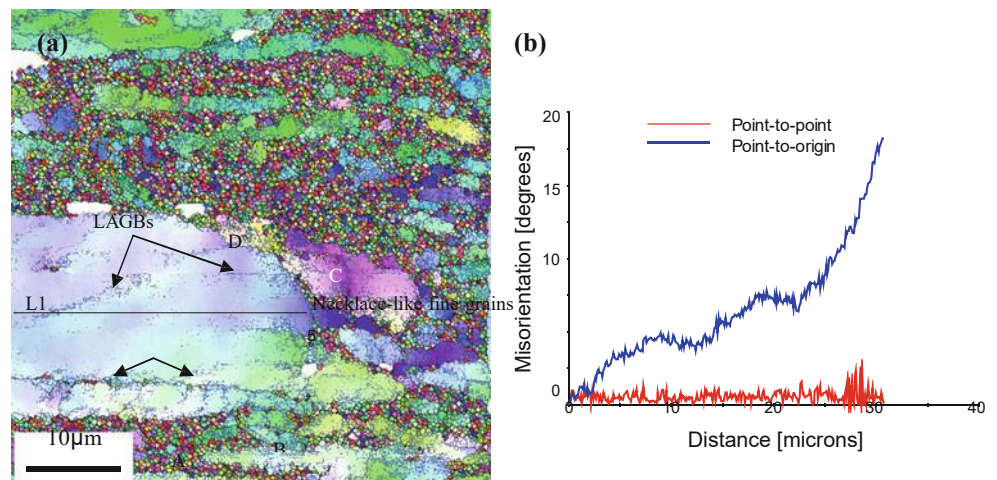


Fig. 6 Microhardness distribution in CP Ti before HPT and after HPT in the LP and TP

Fig. 7 a EBSD orientation maps showing very limited deformation substructures in coarse grains (3 mm from disk center in the longitudinal plane (RD–ND) after 5 turns of HPT). b Misorientation profile along L1 in Fig. 7a (from left to right) showing point to origin (accumulated) misorientation and point to point misorientation with distance



the imposed plastic strain so that dynamic recovery of the dislocation structures in these grains is fairly rapid. Figure 7b shows the misorientation profile along L1 in Fig. 7a. Along the direction of L1, the point-to-point misorientation generally remains below 2.5° , which indicates that cell blocks have been formed mainly in this coarse grain. The accumulated misorientation (point to origin) increases progressively to 18.2° over 30.7 μm , which indicates that the misorientation gradient is quite low. These results suggest that the coarse grains are unfavorably oriented for deformation under the imposed stress state during HPT. This means severe shear mainly takes place in fine grains which in turn develop into even smaller new grains. Moreover, the morphology and alignment of the newly-formed grains in Fig. 7a (marked by A and B) are obviously derived from the coarse grains and some new grains or subgrains (marked by C and D) are present at the “parent” grain boundaries of the coarser grains. Some new grains formed along the LAGBs segments inside coarse grains tend to form necklace-like configuration (marked in Fig. 7a). The necklace-like configurations of fine grains observed in this study (Figs. 2 b, c, 7a) share some similarities with the grain structures observed in the shear zone of an equal channel angular pressing (ECAP) die interrupted during the 4th pass, which was studied in detail by some of the present authors [13]. In that ECAP study, the microstructure was shown to be heterogeneous with grains of sizes between 200 nm and 14 μm coexisting. These inhomogeneous, necklace-like configurations of fine grains are thought to be caused by continuous dynamic recrystallization (CDRX) in CP Ti [13]. CDRX is a recovery dominated process and proceeds by continuous absorption of dislocations in LAGBs which eventually results in the formation of new grains with HAGBs [29]. It appears, therefore, that the refinement process is analogous to hcp metals processed by ECAP where new grains form from the evolution of LAGBs and the continuous formation of these fine grains gradually consumes the larger grains in subsequent passes [30].

Conclusions

- (1) CP Ti produces a heterogeneous microstructure when processing by HPT with arrays of nanocrystalline grains (100 nm) interspersed with much coarser grains (*1–30 μm).
- (2) Tensile $\{10\bar{1}2\}$ twins were observed in the center of the disk after the first turn of HPT processing but the fraction of twins was suppressed in the outer part of the disk during the first turn and during subsequent turns.
- (3) The microhardness near the disk center increases with increasing HPT turns and the hardness after 5 turns is reasonably homogeneous at radial positions [1 mm.

- (4) By analogy with an earlier study on ECAP processed CP Ti, the mechanism of grain refinement appears to be caused by dynamic recrystallization and the continuous formation of a necklace-like array of fine grains gradually consumes the larger grains in subsequent passes.

Acknowledgements This study was supported by the Research Council of Norway under the NANOMAT program (Contract No. 182000/S10) and the National Science Foundation of the United States (Grant No. DMR-0855009) (TGL). Mr Jiuwen Zhang (University of Southampton) is gratefully acknowledged for performing some of the HPT processing.

References

1. Horita Z, Smith DJ, Furukawa M, Nemoto M, Valiev RZ, Langdon TG (1996) *J Mater Res* 11:1880
2. Oh-ishi K, Horita Z, Smith DJ, Valiev RZ, Nemoto M, Langdon TG (1999) *J Mater Res* 14:4200
3. Zhao YH, Liao XZ, Zhu YT, Horita Z, Langdon TG (2005) *Mater Sci Eng A* 410–411:188
4. Zhilyaev AP, Langdon TG (2008) *Prog Mater Sci* 53:893
5. Wei Q, Zhang HT, Schuster BE, Ramesh KT, Valiev RZ, Kecskes LJ, Dowding RJ, Magness L, Cho K (2006) *Acta Mater* 54:4079
6. Čížek J, Procházka I, Smola B, Stulíková I, Kužel R, Matěj Z, Cherkaska V, Islamgaliev RK, Kulyasova O (2007) *Mater Sci Eng A* 462:121
7. Todaka Y, Sasaki J, Moto T, Umemoto M (2008) *Scripta Mater* 59:615
8. Islamgaliev RK, Kazyhanov VU, Shestakova LO, Sharafutdinov AV, Valiev RZ (2008) *Mater Sci Eng A* 493:190
9. Todaka Y, Umemoto M, Yamazaki A, Sasaki J, Tsuchiya K (2008) *Mater Trans* 49:47
10. Edalati K, Matsubara E, Horita Z (2009) *Metall Mater Trans A* 40:2079
11. Wang YB, Louie M, Cao Y, Liao XZ, Li HJ, Ringer SP, Zhu YT (2010) *Scripta Mater* 62:214
12. Bonarski BJ, Schaffler E, Mingler B, Skrotzki W, Mikulowski B, Zehetbauer MJ (2008) *J Mater Sci* 43:7513
13. Chen YJ, Li YJ, Walmsley JC, Dumoulin S, Roven HJ (2010) *Metall Mater Trans* 41A:787
14. Stolyarov VV, Zhu YT, Lowe TC, Valiev RZ (2001) *Mater Sci Eng A* 303:82
15. Valiev RZ, Semenova IP, Latysh VV, Rack H, Lowe TC, Petruzelka J, Dluhos L, Hrusak D, Sochova (2008) *J Adv Eng Mater* 10:B15
16. Vorhauer A, Pippin R (2004) *Scripta Mater* 51:921
17. Serra A, Pond RC, Bacon DJ (1991) *Acta Metall Mater* 39:469
18. Yapici GG, Karaman I, Luo ZP (2006) *Acta Mater* 54:3755
19. Shin DH, Kim I, Kim J, Kim YS, Semiatin SL (2003) *Acta Mater* 51:983
20. Li YJ, Chen YJ, Walmsley JC, Mathiesen RH, Dumoulin S, Roven HJ (2010) *Scripta Mater* 62:443
21. Zhao X, Fu W, Yang X, Langdon TG (2008) *Scripta Mater* 59:542
22. Zhang JW, Gao N, Starink MJ (2010) *Mater Sci Eng A* 527:3472
23. Estrin Y, Molotnikov A, Davies CHJ, Lapovok R (2008) *J Mech Phys Solids* 56:1186
24. Xu C, Horita Z, Langdon TG (2007) *Acta Mater* 55:203
25. Edalati K, Fujioka T, Horita Z (2009) *Mater Trans* 50:44

-
26. Kawasaki M, Figueiredo RB, Langdon TG (2011) *Acta Mater* 59:308
 27. Edalati K, Horita Z, Langdon TG (2009) *Scripta Mater* 60:9
 28. Chen YJ, Li YJ, Walmsley JC, Dumoulin S, Roven HJ (2011) *Scripta Mater* 64:904
 29. Al-Samman T, Gottstein G (2008) *Mater Sci Eng A* 490:411
 30. Figueiredo RB, Langdon TG (2010) *J Mater Sci* 45:4827. doi: [10.1007/s10853-010-4589-y](https://doi.org/10.1007/s10853-010-4589-y)